RSC Advances

Cite this: *RSC Advances*, 2012, **2**, 3361–3366

www.rsc.org/advances

PAPER

Surface charge transfer doping of germanium nanowires by MoO_3 deposition

Lin-Bao Luo,*[a] Tsz-Wai Ng,[b] Hao Tang,[b] Feng-Xia Liang,[b] Yu-Cheng Dong,[b] Jian-Sheng Jie,*[a] Chun-Yan Wu,[a] Li Wang,[a] Zhi-Feng Zhu,[a] Yong-Qiang Yu[a] and Qiang Li[a]

Received 9th December 2011, Accepted 1st February 2012
DOI: 10.1039/c2ra01269c

We report on the surface transfer p-type doping of germanium nanowires (GeNWs) *via* MoO_3 thin film deposition. The GeNWs studied were prepared by a conventional thermal evaporation approach. Electrical property analysis shows that the conductance, hole mobility and concentration were all prominently enhanced after MoO_3 thin film coating. Such a remarkable surface doping effect can be attributed to the surface charge transfer at the GeNWs/MoO_3 interface, which is verified by *in situ* XPS analysis of GeNWs as a function of increasing MoO_3 coverage. Further hole mobility and concentration evolution study of MoO_3/GeNWs reveals that the GeNWs embedded in the MoO_3 layer can retain their electrical property after storage in air for 3 months. The generality of the above results suggests that the charge transfer doping *via* surface deposition has great potential in GeNW-based nanoelectronic devices and may also be applicable to the modulation of other semiconductor nanostructures.

Introduction

In the last decade, one-dimensional (1D) semiconductors, such as group IV, III–V, and II–VI compounds nanowires (NWs), have been actively investigated in an effort to utilize them for various advanced applications, *e.g.*, field-effect transistors (FETs),[1,2] logic circuits,[3,4] light-emitting diodes (LEDs),[5,6] solar cells,[7,8] photodetectors,[9,10] and biological or chemical sensors.[11,12] In particular, elementary semiconductor NWs, such as silicon NWs (SiNWs) and germanium NWs (GeNWs), have exhibited unique electrical properties with respect to their bulk counterparts and good compatibility with the existing semiconductor technology. SiNWs and GeNWs are the most promising building blocks for future functional devices at the nanoscale level.[13]

Compared with Si, Ge has higher electron and hole mobilities, a lower intrinsic resistivity and larger Bohr exciton radius.[13,14] This unparalleled superiority, combined with the convenient synthesis renders GeNWs appealing candidates for low drive voltage, high drive current and high-speed electronic devices.[15,16] Nonetheless, undeniably, due to the huge surface to volume ratio, the electrical properties of GeNWs are highly dependent on the surrounding atmosphere and difficult to control. On the other hand, GeNWs can easily get oxidized in ambient conditions, forming a water soluble GeO_2 sheath surrounding the NW.[17] This feature makes GeNWs highly unstable and thereby constitutes the major obstacle to their wide application in optoelectronic devices.[18] Exploration of effective ways to rationally control the electrical properties of GeNWs with favorable stability is thus highly desirable.

The development of the surface charge transfer technique holds great promise. As established previously, surface doping is completely different from the traditional volume doping method in that it can allow direct charge transfer from one material to another by virtue of their remarkable differences in work functions.[19] Moreover, compared with the traditional doping method by intentionally introducing impurity atoms into the crystal lattice, this surface-induced doping approach is relatively convenient and can allow rational tailoring of the electrical properties of semiconductor without damaging the interior structures. In this study, we present an attempt to dope GeNWs *via* a surface charge transfer approach. The doping effect of the GeNWs through MoO_3 coating were evaluated by characterizing single GeNW-based FETs and the surface charge transfer at MoO_3/GeNW interface was probed by *in situ* X-ray photoelectron spectroscopy (XPS). The observed considerable injection of holes from MoO_3 into GeNW, along with the long-term stability suggests that the surface charge transfer doping is applicable to the modulation of the electrical properties of other semiconductor nanostructures.

Experiment

Synthesis and characterization of germanium nanowires

The fabrication of GeNWs was carried out on a three zone horizontal tube furnace.[19] Briefly, 2 g of germanium powder (99.99%, Sigma-Aldrich Co.) was placed in an alumina boat at the center of the tube furnace. Then, a piece of thermally oxide p^+-Si wafer (300 nm SiO_2) loaded with a very thin layer of gold

[a]*School of Electronic Science and Applied Physics, Hefei University of Technology, Hefei, Anhui, 230009, P. R. China. E-mail: luolb@hfut.edu.cn (L. B. Luo); jsjie@hfut.edu.cn (J. S. Jie)*
[b]*Department of Physics and Materials Science, City University of Hong Kong, Kowloon, Hong Kong SAR, P. R. China*

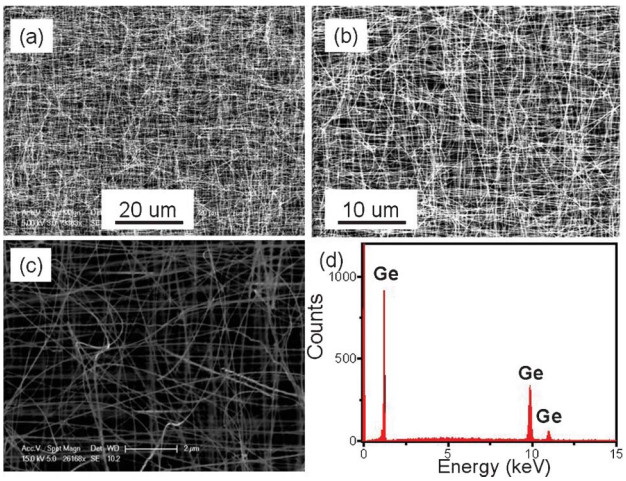

Fig. 1 (a–c) SEM images of the GeNWs at different magnification. (d) The corresponding EDX spectrum.

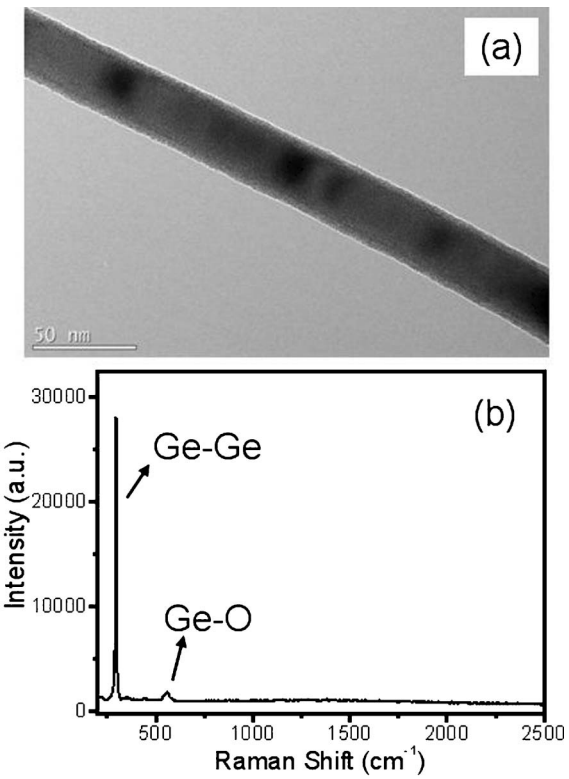

Fig. 2 (a) A TEM image of a typical GeNW. (b) The Raman spectrum of GeNWs showing the presence of both Ge and Ge oxide.

nanoparticles was placed in the downstream direction. After the tube was pumped down to a pressure of 1×10^{-2} mbar, high purity mixed gas of H_2/Ar (5/95%) was introduced into the tube at a rate of 20 sccm. The germanium powder was increased to 900 °C at a rate of 15 °C min^{-1} and the Si substrate to 450 °C at a rate of 7.5 °C min^{-1}, and kept for about 1 h. Throughout the growth process, the system was maintained at 200 mbar. Finally, the product was collected from the SiO_2/Si substrate after the system was allowed to cool down to ambient temperature. The

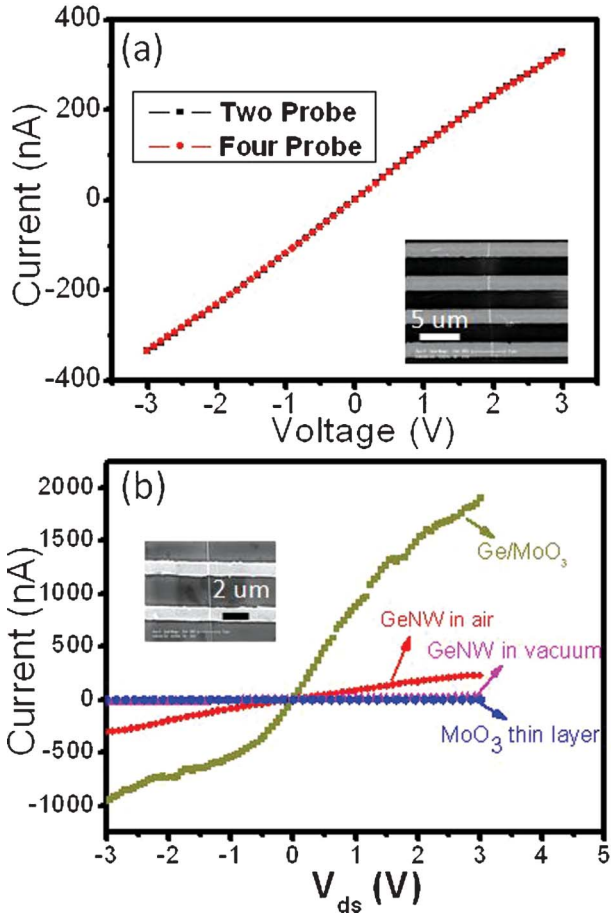

Fig. 3 (a) *I–V* curves measured in both two-probe and four-probe configurations; inset shows four parallel Ti/Au electrodes bridged by an individual GeNW. (b) Conductance of GeNW in air, vacuum, GeNW coated with MoO_3 (GeNW/MoO_3), and MoO_3 thin film, inset is the SEM image of a typical GeNW-FET.

morphologies and crystal structures were investigated by field-emission scanning electron microscopy (FESEM, Philips XL 30 FEG) and transmission electron microscopy (TEM, Philips CM20, operating at 200 KV). The elemental compositions were analyzed by energy dispersive spectroscopy (EDS) attached to the FESEM system. The Raman scattering measurements were performed on a Renishaw 2000 spectrometer with incident 633 nm laser.

Device fabrication and measurement

The fabrication of single-GeNW based FETs followed a standard photolithography process. Briefly, the as-prepared GeNWs were first scraped from the Si substrate and immersed into an absolute alcohol solution *via* ultrasonication. The resulting NWs suspension was then spread onto a 500 nm SiO_2/p^+-Si substrate. Photolithography (Mask aligner: Karl Suss MJB-3) and a lift-off process were employed to define the Ti (2 nm)/Au (80 nm) source and drain electrodes with 2 μm finger spacing on the individual GeNWs. Afterwards, 100 nm Al was deposited onto the back of the p^+-Si substrate, which serves as the back gate electrode. To study the effects of surface transfer doping, MoO_3 thin film was directly deposited onto the GeNW-based FETs

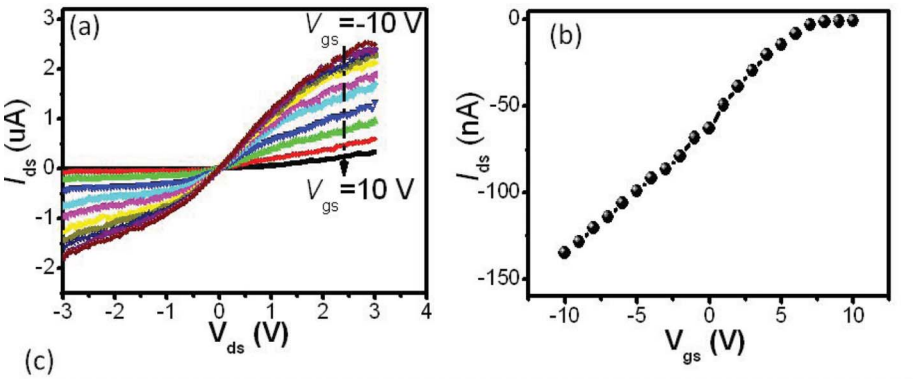

(c)

	GeNW in air	GeNW in vacuum	GeNW/MoO_3
Hole mobility (cm^2/Vs)	17.4	7.6	45.3
Hole concentration (cm^{-3})	2.1×10^{17}	3.1×10^{16}	5.8×10^{17}
Resistivity (Ω·cm)	1.7	26.5	0.24

Fig. 4 (a) I_{ds}–V_{ds} curve of GeNW after deposition of MoO_3, under different gate voltages. (b) Corresponding transport characteristics at V_{ds}= −0.1 V. (c) Table of electrical properties of GeNW in air, vacuum and with a layer of MoO_3 thin film.

through a thermal evaporator. The evaluation of the GeNW FETs was carried out on a semiconductor characterization system (Keithley 4200-SCS).

XPS analysis

XPS analysis was performed *in situ* using a VG ESCALAB 220i-XL surface analysis system equipped with a monochromatic Al Kα X-ray (1486.6 eV) source. The analysis system is composed of interconnected analysis, coating and preparation chambers with vacuum pressures of 3×10^{-10}, 5×10^{-10}, and 3×10^{-7} Torr, respectively. The MoO_3 layer was deposited stepwise by thermal evaporation inside the deposition chamber at pressure of around 1×10^{-9} Torr. The freshly prepared samples were transferred to the analysis chamber for *in situ* XPS study without vacuum break.

Results and discussion

The general overview FESEM image in Fig. 1(a) shows that the product obtained by evaporating pure Ge powder is composed of network-like NWs. The GeNWs are up to tens of micrometres in length, and exhibit high abundance and purity without any appreciable by-products. Further magnified FESEM and TEM images in Fig. 1(b) and (c) reveal that the NWs are comparatively uniform along the whole length with diameter in the range 40–90 nm. In addition to Ge which is found in the elemental composition analysis shown in Fig. 1(d), a layer of amorphous germanium oxide thin film (GeO_2 or GeO) was observed on the GeNWs surface (*cf.* the XPS result in Fig. 6). This species, according to the early work, results from the rapid oxygen oxidation when exposed to air, which is usually unavoidable during NWs preparation.[20] In fact, the presence

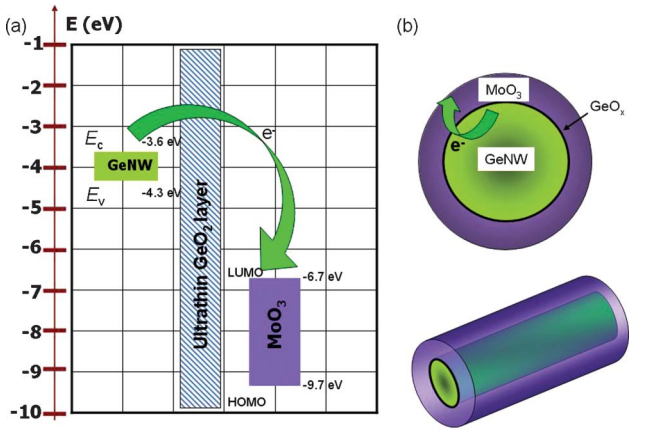

Fig. 5 (a) A schematic illustration of the electron injection from GeNW to MoO_3. (b) An electronic structures diagram of both GeNW and MoO_3.

of a thin Ge oxide layer is also confirmed by the Raman spectrum shown in Fig. 2(b).[21]

Fig. 3(a) shows the typical *I*–*V* curves of a single GeNW acquired from both two-probe and four-probe approaches. The linear curves throughout the voltage measurement range reveal the good ohmic contact between the electrodes and GeNW. The resistance of the NW is calculated to be 8.9×10^6 Ω and the contact resistance, namely the difference between the two-probe and four-probe resistance is 4.1×10^4 Ω. In light of the relatively low contact resistance, probably due to the matched work function,[22] a two-probe method is used in the following experiments. The inset in Fig. 3(b) shows a typical FESEM image of the GeNW FET after 20 nm MoO_3 deposition, in which two

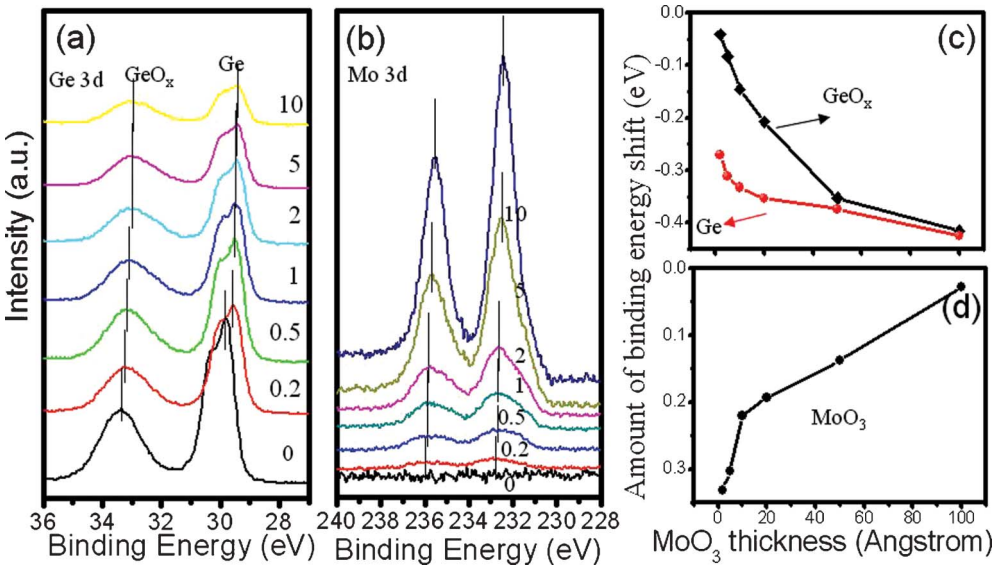

Fig. 6 XPS spectra of Ge 3d (a) and Mo 3d (b) peaks for GeNWs coated with MoO_3 of increasing thickness of 0, 0.2, 0.5, 1, 2, 5 and 10 nm. The binding energy shift of Ge 3d for GeNWs (c) and Mo 3d for MoO_3 (d) with increasing MoO_3 coverage. The shift of the binding energy confirms the surface charge transfer at the GeNWs and MoO_3 interface.

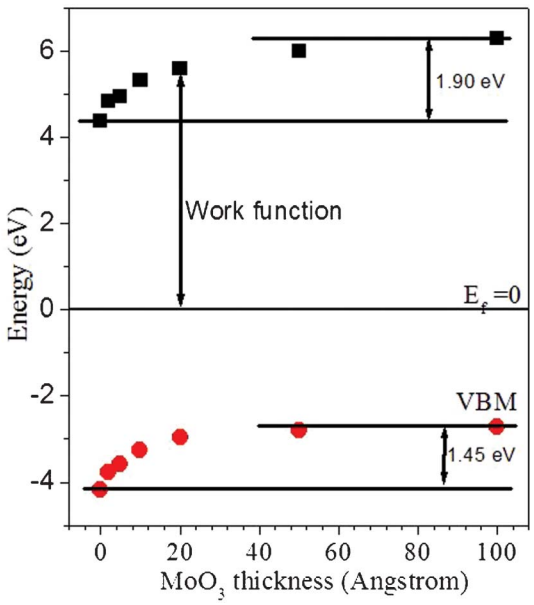

Fig. 7 The energy level alignment of MoO_3 as a function of increasing MoO_3 thickness.

parallel gold electrodes are crossed by an individual GeNW. The effective gate length is 2.5 μm and the diameter of the NW is 80 nm. Fig. 3(b) plots I_{ds} *vs.* V_{ds} curves of a pure MoO_3 thin layer and GeNW in air, at vacuum and after MoO_3 coating. Among the four structures, MoO_3 shows the lowest conductance, while the GeNW has higher conductance in air than when in a vacuum, mainly due to the ambient effect. Interestingly, after coating with a 20 nm MoO_3 thin layer, the as-obtained GeNW/MoO_3 structure shows the highest conductance. These results suggest that the substantial increase of the conductance for the MoO_3-coated GeNW (GeNW/MoO_3) cannot be solely attributed to the conductance enhancement of the MoO_3 coating layer. As we will discuss later, the surface charge transfer between the MoO_3 and GeNW interface is likely responsible for this phenomenon.

Further electrical transport characterization indicates that the undoped GeNWs without MoO_3 coating shows weak p-type semiconductivity (data not shown). This behavior is attributed to the presence of a huge quantity of surface dangling bonds that can lead to the formation of an acceptor level slightly above the valance band maximum.[23] In contrast, the p-type conductivity of the GeNW is remarkably enhanced after coating with MoO_3 thin layer. Fig. 4(a) and (b) depict the transport characteristics of the GeNW FET after MoO_3 coating. The device exhibits a typical behavior of a p-channel semiconductor FET, with a hole mobility and concentration of 45.3 $cm^2\ V^{-1}\ s^{-1}$ and 5.8 × $10^{17}\ cm^{-3}$, respectively. A comparison of the hole mobility, hole concentration and resistivity of the GeNW in air, a vacuum and after MoO_3 deposition is summarized in Fig. 4(c). It is worth noting that owing to oxygen and water molecules absorption on the surface dangling bonds, an acceptor level above the valence band was formed, contributing to the p-type conductivity of the GeNW in air. Desorption of these surface molecules in a vacuum leads to the decrease of the hole concentration. As a result, the resistivity of the GeNW increases by nearly one order of magnitude in a vacuum. On the other hand, the MoO_3 coating on the GeNW results in the increase of both the hole mobility and the hole concentration. Consequently, the GeNW resistivity decreases by one order of magnitude with respect to that in air. The enhanced carrier mobility of GeNW after MoO_3 coating is probably due to the reduced carrier scattering as a consequence of surface oxygen and water molecules desorption, as well as the effective surface passivassion.[24,25] As for the increase in hole concentration, it is assumed to be associated with the mutual surface charge transfer between the GeNW and MoO_3 thin layer due to their differences in work function, which will be verified by the *in situ* XPS analysis result later on.

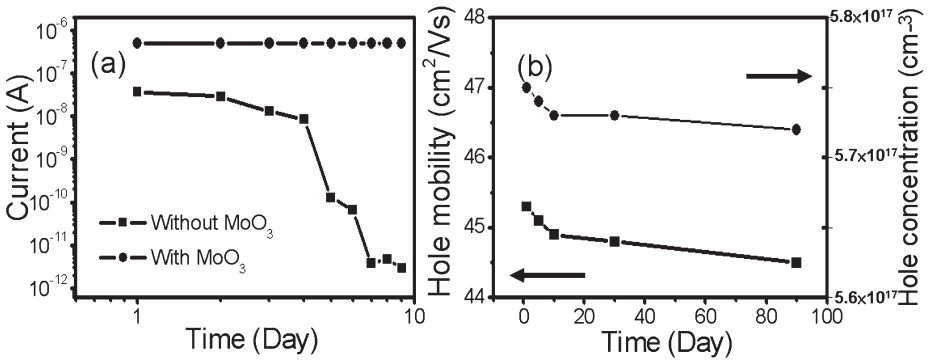

Fig. 8 (a) Current evolution of a GeNW with and without MoO_3 thin film deposition. (b) Hole mobility and concentration evolution of the MoO_3-coated GeNW as a function of time.

Previously, it has been reported that MoO_3 has a very low lowest unoccupied molecular orbital (LUMO) value of −6.7 eV and highest occupied molecular orbital (HOMO) value of −9.7 eV,[26] signifying that the work function of MoO_3 is comparatively larger than the majority of other materials including organic and inorganic semiconductors, thereby favoring holes injection from MoO_3 to the other semiconductors, which render it an effective hole injector in organic LEDs and organic FETs.[27,28] In our case, the huge difference in work functions between MoO_3 and GeNW also accounts for the enhanced p-type conductivity in GeNW after MoO_3 coating. As we can see in Fig. 5(a), the conduction band minimum (E_c) and the valence band maximum (E_v) of the GeNW are located at −3.6 and −4.3 eV, respectively. The Fermi level is above both the HOMO and LUMO of MoO_3. As a result, electrons will transfer spontaneously from GeNW to MoO_3 (Fig. 5(b)), giving rise to the increase in hole concentration within the GeNW. It is noteworthy that although an ultrathin GeO_2 sheath is often observed on the outside of the GeNWs, it is too thin to block the electron transfer *via* direct tunneling. Moreover, similar electron transfer from GeO_2 to MoO_3 was also investigated in the XPS analysis below.

As a matter of fact, the observed surface charge transfer doping effect was experimentally verified by XPS spectrum evolution of Ge 3d and Mo 3d with increasing nominal MoO_3 coverage, as shown in Fig. 6(a). It can be clearly visualized that prior to MoO_3 coating, the spectrum of Ge 3d is mainly composed of two Ge 3d peaks centered at binding energy of 29.84 and 33.32 eV, corresponding to Ge and GeO_2, respectively. When the MoO_3 thin layer is deposited stepwise, a gradual shift of Ge 3d towards low binding energy is observed for both peaks. Fig. 6(c) plots the binding energy shift as a function of MoO_3 layer thickness, in which a total shift of about 0.43 eV for Ge and 0.42 eV for GeO_2 is observed as MoO_3 thickness increase from 0 to 10 nm. This binding energy shift corresponds to the upward energy level bending from bulk to interface, indicating that GeNW loses electrons near the heterojunction interface. The surface charge transfer effect at the GeNW/MoO_3 interface is corroborated by the corresponding Mo 3d spectrum evolution as well. As shown in Fig. 6(b), with the increase in MoO_3 thickness, the binding energy of Mo 3d shifts downwards by 0.33 eV; this shift suggests that the electrons were injected from the GeNW to MoO_3, in good agreement with the enhanced p-type electrical conduction behavior.

The charge transfer at the interface is also verified by the formation of an interface dipole. Fig. 7 plots the evolution of work function and VBM (*i.e.*, the band bending) of MoO_3 as a function of MoO_3 layer thickness, from which one can see that as the dopant layer thickness increases from 0 to 100 Å, both the work function and VBM increase. Notably, a careful comparison of both values concludes that the change in work function is always larger than that of the band bending. This result suggests the existence of an interfacial dipole at the MoO_3/GeNW interface, thus corroborating the electron transfer from GeNW to MoO_3 at the contacting junction, considering the fact that the overall change in work function includes the contribution from both band bending and interfacial dipole.[29,30]

It is worth mentioning that the MoO_3 thin layer can not only serve as an effective hole injector, but also help prevent the GeNWs from getting oxidized when exposed in ambient conditions, which is often observed on GeNWs and responsible for the degeneration of their electrical properties.[31] As depicted in Fig. 8(a), the GeNW without MoO_3 thin layer coverage can get easily oxidized and its electrical conduction attenuates at a considerable pace in less than 1 week. However, the deposition of a MoO_3 thin layer can act as a protective layer and greatly restrict such an oxidization process. Fig. 8(b) shows the hole mobility and the hole concentration of a 20 nm MoO_3-coated GeNW FET as a function of exposure duration, from which one can see that the hole mobility decreases slightly from 45.3 to 44.5 $cm^2\ V^{-1}\ s^{-1}$, and hole concentration decreases slightly from 5.75×10^{17} to 5.72×10^{17} cm^{-3} after storage in air for 3 months. The change in the device parameters is less than 2%, which unambiguously demonstrates that the GeNWs embedded in the MoO_3 thin layer are extremely stable, greatly facilitating their applications in future nanoelectronic devices.

In summary, we have presented a surface transfer approach to the effective p-type doping of GeNWs *via* MoO_3 thin film coating. The GeNWs studied were prepared by a conventional thermal evaporation approach. The electrical property study of the single GeNW-based field effect transistor and *in situ* XPS analysis of GeNWs as a function of increasing MoO_3 coverage support the supposition that a considerable quantity of holes was transferred from MoO_3 to GeNWs due to their difference in work function. Finally, the long-term electrical property study of the GeNW reveals that the hole mobility and concentration remain almost the same. The generality of this work demonstrates that surface

transfer doping is an effective method to tailor the electrical property of GeNWs.

Acknowledgements

This work was supported by the National Natural Science Foundation of China (Nos.60806028, 61106010, 21101051, 20901021), the Program for New Century Excellent Talents in University of the Chinese Ministry of Education (NCET-08-0764), the Major Research Plan of the National Natural Science Foundation of China (No. 91027021) and the Fundamental Research Funds for the Central Universities.

References

1 J. Golberger, A. I. Hochbaum, R. Fan and P. D. Yang, *Nano Lett.*, 2006, **6**, 973–977.
2 Y. Cui, Z. Zhong, D. Wang, W. U. Wang and C. M. Lieber, *Nano Lett.*, 2003, **3**, 149–152.
3 Y. Huang, X. F. Duan, Y. Cui, L. J. Lauhon, K. H. Kim and C. M. Lieber, *Science*, 2001, **294**, 1313–1317.
4 W. I. Park, J. S. Kim and H. J. Lee, *Nano Lett.*, 2005, **17**, 1393–1397.
5 X. F. Duan, Y. Huang, R. Agarwal and C. M. Lieber, *Nature*, 2003, **421**, 241–245.
6 Y. Huang, X. F. Duan and C. M. Lieber, *Small*, 2005, **1**, 142–147.
7 T. J. Kempa, B. Z. Tian, D. R. Kim, J. S. Hu, X. L. Zheng and C. M. Lieber, *Nano Lett.*, 2008, **8**, 3456–3460.
8 M. Zukalova, A. Zukal, L. Kavan, M. K. Nazeeruddin, P. Liska and M. Gratzel, *Nano Lett.*, 2005, **5**, 1789–1792.
9 L. Rigutti, M. Tchernycheva, A. D. Bugallo, G. Jacopin, F. H. Julien, L. F. Zagonel, K. March, O. Stephan, M. Kociak and R. Songmuang, *Nano Lett.*, 2010, **10**, 2939–2943.
10 L. B. Luo, J. S. Jie, Z. H. Chen, X. J. Zhang, X. Fan, G. D. Yuan, Z. B. He, W. F. Zhang, W. J. Zhang and S. T. Lee, *J. Nanosci. Nanotech.*, 2009, **9**, 6298–7304.
11 Y. Cui, Q. Q. Wei, H. K. Park and C. M. Lieber, *Science*, 2001, **293**, 1289–1292.
12 L. B. Luo, J. S. Jie, W. F. Zhang, Z. B. He, J. X. Wang, G. D. Yuan, W. J. Zhang, L. C. M. Wu and S. T. Lee, *Appl. Phys. Lett.*, 2009, **94**, 193101–3.
13 B. S. Kim, T. W. Koo, J. H. Lee, D. S. Kim, Y. C. Jun, S. W. Hwang, B. L. Choi, E. K. Lee, J. M. Kim and D. M. Whang, *Nano Lett.*, 2009, **9**, 864–869.
14 P. Nguyen, H. T. Ng and M. Meyyappan, *Adv. Mater.*, 2005, **17**, 549–553.
15 P. Logan and X. H. Peng, *Phys. Rev. B*, 2009, **80**, 115322.
16 R. P. Prasankumar, S. Choi, S. A. Trugman, S. T. Picraux and A. J. Taylor, *Nano Lett.*, 2008, **8**, 1619–1624.
17 S. J. Sze, *Physics of Semiconductor Devices*, 2nd ed.1981, Wiley, New York.
18 X. Y. Wu, J. S. Kulkarni, G. Collins, N. Petkov, D. Almecija, J. J. Boland, D. Erts and J. D. Holmes, *Chem. Mater.*, 2008, **20**, 5954–5967.
19 J. Ristein, *Science*, 2006, **313**, 1057–1058.
20 D. W. Wang, Y. L. Chang, Z. Liu and H. J. Dai, *J. Am. Chem. Soc.*, 2005, **127**, 11871–11875.
21 N. Fukata, K. Sato, M. Mitome, Y. Bando, T. Sekiguchi, M. Kirkham, J. I. Hong, Z. L. Wang and R. L. Snyder, *ACS Nano*, 2010, **4**, 3807–3816.
22 Q. X. Tang, Y. H. Tong, W. P. Hu, Q. Wan and T. Bjornholm, *Adv. Mater.*, 2010, **21**, 4234–4237.
23 L. B. Luo, X. B. Yang, F. X. Liang, J. S. Jie, C. Y. Wu, L. Wang, Y. Q. Yu and Z. F. Zhu, *J. Phys. Chem. C*, 2011, **115**, 24293–24299.
24 C. S. Guo, L. B. Luo, G. D. Yuan, X. B. Yang, R. Q. Zhang, W. J. Zhang and S. T. Lee, *Angew. Chem., Int. Ed.*, 2009, **48**, 9896–9900.
25 J. S. Jie, W. J. Zhang, K. Q. Peng, G. D. Yuan, C. S. Lee and S. T. Lee, *Adv. Funct. Mater.*, 2008, **18**, 3251–3257.
26 M. Kroger, S. Hamwi, J. Meyer, T. Riedl, W. Kowalsky and A. Kahn, *Org. Electron.*, 2009, **10**, 932–938.
27 J. Meyer, R. Khalandovsky, P. Gorrn and A. Kahn, *Adv. Mater.*, 2011, **23**, 70–73.
28 H. B. Wang, Z. T. Liu, M. F. Lo, T. W. Ng, C. S. Lee, D. H. Yan and S. T. Lee, *J. Appl. Phys.*, 2010, **107**, 024510–3.
29 H. Ishiii, K. Sugiyama, E. Ito and K. Seki, *Adv. Mater.*, 1999, **11**, 605.
30 D. C. Qi, W. Chen, X. Y. Gao, L. Wang, S. Chen, K. P. Loh and A. T. S. Wee, *J. Am. Chem. Soc.*, 2007, **129**, 8084.
31 R. H. Kinston, *Semiconductor Surface Physics*, University of Pennsylvania Press, Philadelphia, 1957.

